

# Programmable XY-type couplings through parallel spin-dependent forces on the same trapped ion motional modes

Nikhil Kotibhaskar, Chung-You Shih, Sainath Motlakunta,  
Anthony Vogliano, Lewis Hahn, Yu-Ting Chen, and Rajibul Islam  
*Institute for Quantum Computing and Department of Physics and Astronomy,  
University of Waterloo, Waterloo, ON, N2L 3G1, Canada*  
(Dated: July 12, 2023)

We propose and experimentally demonstrate an analog scheme for generating XY-type ( $J_{ij}^x \sigma_x^i \sigma_x^j + J_{ij}^y \sigma_y^i \sigma_y^j$ ) Hamiltonians on trapped ion spins with independent control over the  $J_{ij}^x$  and  $J_{ij}^y$  terms. The Ising-type interactions  $\sigma_x^i \sigma_x^j$  and  $\sigma_y^i \sigma_y^j$  are simultaneously generated by employing two spin-dependent forces operating in parallel on the same set of normal modes. We analytically calculate the region of validity of this scheme, and provide numerical and experimental validation with  $^{171}\text{Yb}^+$  ions. This scheme inherits the programmability and scalability of the Ising-type interactions with trapped ions that have been explored in numerous quantum simulation experiments. Our approach extends the capabilities of existing trapped ion quantum simulators to access a large class of spin Hamiltonians relevant for exploring exotic quantum phases such as superfluidity and spin liquids.

Trapped ions are ideal quantum simulators of interacting spin systems [1, 2] due to their tunable long-range interactions [3–5], long coherence times [6] and high fidelity quantum state preparation and measurement [7]. Interacting spin models illuminate a large variety of many-body phenomena such as quantum magnetism and phase transitions, spin liquids, superconductivity, and superfluidity [8, 9]. Spins encoded in the internal degrees of freedom (such as hyperfine states) of individual trapped ions can interact via off-resonant excitation of their collective phonon modes through laser-driven spin-dependent dipole forces. By varying the laser parameters, long-range and tunable Ising-type interactions have been experimentally demonstrated and used in a large number of quantum simulations to explore both equilibrium and dynamic phenomena. Further, it has been proposed that the inherent long-range Coulomb interactions can be used to realize an arbitrarily programmable, all-to-all connected Ising spin system [10, 11].

Existing proposals to simulate models that capture symmetries and phenomena beyond the reach of Ising models, such as XY and Heisenberg models, are either experimentally challenging or unfeasible, or limited in their applicability and tunability. For example, non-local propagation of spin correlations [12, 13] and many-body localization [14] were studied, on an effective XY-Hamiltonian, by applying a large transverse magnetic field to the Ising Hamiltonian. The transverse field restricts the Hilbert space contributing to the spin dynamics and results in an effective XY Hamiltonian only at discrete times [12, 15]. The above approach also breaks down for long evolution times [15], and does not allow the simulation of the anisotropic XY model (i.e., interactions of the form  $J_{i,j}^x \sigma_x^i \sigma_x^j + J_{i,j}^y \sigma_y^i \sigma_y^j$  with  $J_{i,j}^x \neq J_{i,j}^y$ , where  $\sigma_{x(y)}^i$  are the usual spin-1/2 Pauli matrices). Alternate proposals make use of orthogonal sets [16] of motional modes, with each set mediating an independent Ising term (such as  $\sigma_x^i \sigma_x^j$  or  $\sigma_y^i \sigma_y^j$ ). However, exciting

multiple sets of orthogonal normal modes require additional laser beams, electronic controls, and complex optical design beyond the scope of current experimental setups. Further, this scheme may not produce the same form and range of interactions along different spin axes [1], limiting the usefulness of such simulations.

Here, we demonstrate the creation of XY-type interactions, including the anisotropic XY-model, that simulates the equivalent spin dynamics in continuous time (limited by the coherence time of the system), and is readily implemented in existing experimental setups. Our key insight is that the same set of motional modes can mediate both  $\sigma_x^i \sigma_x^j$  and  $\sigma_y^i \sigma_y^j$  interactions and the error in the evolution can be made negligible with the proper choice of the applied spin-dependent forces. We experimentally demonstrate the dynamics of two  $^{171}\text{Yb}^+$  ion spins under the simulated XY Hamiltonian and numerically show that the scheme is easily scaled for larger systems.

Spin-spin interactions can be induced [1] between ions by employing spin-dependent forces (SDF) that off-resonantly excite their collective vibrational modes. Such SDFs can be applied using Raman transitions from lasers that are far detuned from unwanted atomic excitation. The Mølmer-Sørensen scheme [5] for generating Ising-type interactions uses an SDF at a frequency  $\mu$  that is generated by simultaneously applying Raman ‘beatnote’ frequencies  $\omega_{\text{hf}} \pm \mu$  (the so-called ‘blue’ and ‘red’ sidebands) [4, 18]. Here,  $\omega_{\text{hf}}$  is the frequency splitting between the two spin states.

Under the rotating wave ( $\omega_{\text{hf}} \gg \mu$ ) and the Lamb-Dicke approximations [1, 18, 19], the spin-phonon Hamiltonian is:

$$H = \sum_i \Omega_i \cos(\mu t + \psi_i) (\delta \vec{k} \cdot \vec{x}_i) \sigma_{\theta_i}^i \quad (1)$$

where,  $\delta \vec{k} \cdot \vec{x}_i = \sum_m \eta_{im} (\hat{a}_m e^{-i\omega_m t} + \hat{a}_m^\dagger e^{i\omega_m t})$ . Here,  $\Omega_i$  is the Rabi frequency at the  $i^{\text{th}}$  ion position,  $\hat{a}_m$  and  $\hat{a}_m^\dagger$  are the phonon annihilation and creation op-

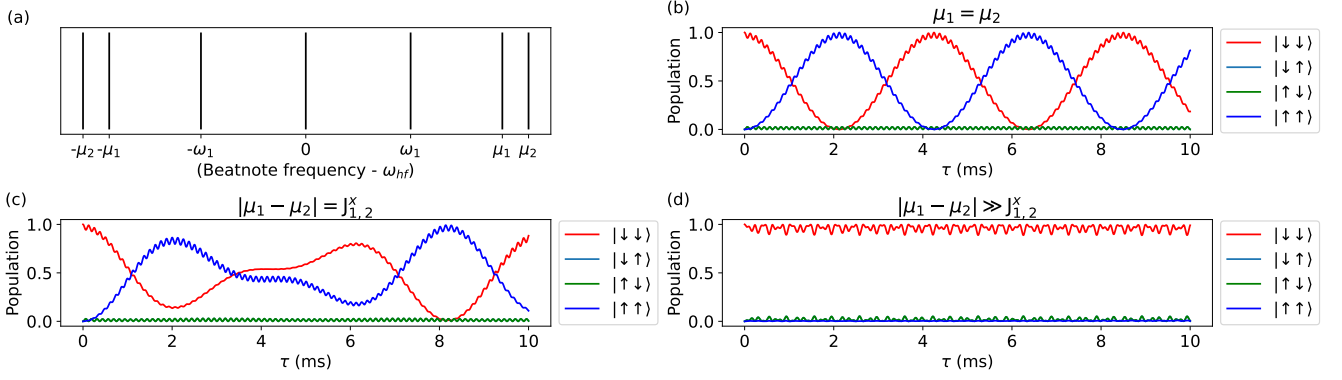


FIG. 1. **Schematic of the protocol and numerical simulation (Eq. (4) with 2 ions and one motional mode at frequency  $\omega_1$ ).** (a) Schematic of the applied beatnotes generating SDFs at frequencies  $\mu_1$  (for coupling to  $\sigma_x$  spin components) and  $\mu_2$  (for coupling to  $\sigma_y$  spin components). The frequency axis is not drawn to scale. The time evolution of the quantum state initialized in  $|\downarrow\downarrow\rangle$ , shown in (b)-(d), are numerically calculated (using the python QuTiP library [17]) from Eq. (4). Probabilities of the four basis states (indicated in the plot legends) are calculated after tracing out the phonon degrees of freedom. Here,  $\omega_1 = 2\pi \times 1.1$  MHz,  $\mu_1 = 2\pi \times 1.108$  MHz,  $\psi_i^x = \psi_i^y = 0$ ,  $\eta_{i1} = 0.0648$ , and  $\Omega_i^x = 2\pi \times 15$  kHz ( $i = 1, 2$ ).  $\Omega_i^x$  is chosen to generate  $J_{12}^x \approx 2\pi \times 60$  Hz (calculated from Eq. (6)) and we truncate the motional Hilbert space to up to four phonons (five levels). (b) Evolution for  $\mu_1 = \mu_2$  and  $\Omega_i^x = \Omega_i^y$  for  $i = 1, 2$ . Since we are effectively applying a single spin-dependent force, the interaction is simply Ising type (with the high-frequency oscillations, also seen in (c)-(d), arising from the off-resonant phonon excitation, i.e., from the first term in the exponent of Eq. (2)). (c) For  $|\mu_1 - \mu_2| \approx J_{12}^x$  and  $\Omega_i^x = \Omega_i^y$  for  $i = 1, 2$ , the resulting dynamics is not pure XY-type due to the last two terms in the exponent of Eq. (5) being non-negligible. (d) For  $|\mu_1 - \mu_2| \gg J_{12}^x$  ( $\mu_2 = 2\pi \times 1.105$  MHz), an effective XY-type Hamiltonian (Eq. (7)) is realized. We set  $\Omega_i^y = 2\pi \times 12.2$  kHz for  $i = 1, 2$  to set  $J_{12}^y = J_{12}^x$  and observe dynamics of the effective XY Hamiltonian (i.e., lack of oscillations between  $|\downarrow\downarrow\rangle$  and  $|\uparrow\uparrow\rangle$ ). In choosing the exact value of  $\Omega_i^y$  here, we use Eq. (6), with an added correction (about 3%) to account for the AC Stark shift arising due to off-resonant excitation of the phonon mode, not considered in Eq. (5).

erators for the  $m^{\text{th}}$  motional mode at frequency  $\omega_m$ . The Lamb-Dicke parameters  $\eta_{im} = b_{im}|\delta\vec{k}|\sqrt{\hbar/2M\omega_m}$  include the normal mode transformation matrix element  $b_{im}$  of the  $i^{\text{th}}$  ion and  $m^{\text{th}}$  normal mode [20]. Where  $\sum_i |b_{im}|^2 = \sum_m |b_{im}|^2 = 1$ ,  $M$  is the mass of the ion and  $\sigma_{\theta_i}^x = \sigma_x^i \cos \theta_i + \sigma_y^i \sin \theta_i$ . The spin phase  $\theta_i$  and the motional phase  $\psi_i$  are determined from the relative phases of the red and blue sidebands [1]. The evolution operator for this Hamiltonian can be found using the Magnus expansion, which terminates after the second term,

$$U(\tau) = \exp \left( -i \int_0^\tau dt H(t) - \frac{1}{2} \int_0^\tau dt_1 \int_0^{t_1} dt_2 [H(t_1), H(t_2)] \right) \\ = \exp \left( \sum_i \hat{\phi}_i(\tau) \sigma_{\theta_i}^i + i \sum_{i < j} \chi_{i,j}(\tau) \sigma_{\theta_i}^i \sigma_{\theta_j}^j \right). \quad (2)$$

In the ‘slow’ regime ( $|\mu - \omega_m| \gg \eta_{im}\Omega_i$ ),  $\hat{\phi}_i(\tau)$  is negligible [4] and  $\chi_{i,j}(\tau)$  in Eq. (2) is dominated by a ‘secular’ term, which grows linearly with  $t$ , giving rise to an effective Hamiltonian,

$$H_{\text{eff}} = \hbar \sum_{i < j} J_{i,j} \sigma_{\theta_i}^i \sigma_{\theta_j}^j \quad (3)$$

where, the Ising coupling,

$$J_{i,j} = \Omega_i \Omega_j \frac{\hbar(\delta\vec{k})^2}{2M} \sum_m \frac{b_{im} b_{jm}}{\mu^2 - \omega_m^2}.$$

Note that, the unitary evolution in Eq. (2) will, in general, include additional AC Stark shifts such as from off-resonant excitation of the ‘carrier’ spin transition from the SDFs (which we did not include in Eq. (1) and (4), as in Refs. [1, 4] for simplicity, but they must be accounted for in experiments).

Multiple SDFs operating in parallel have been theoretically suggested [21] for creating more complex interactions. Recent experiments have used SDFs along two orthogonal modes to generate parallel quantum gates [22]. In our protocol, we apply two SDFs at frequencies  $\mu_1$  and  $\mu_2$  (Fig. 1(a)), with both of them exciting (off-resonantly) the same motional modes. We choose the red and blue sideband phases to generate a spin phase of 0 (corresponding to  $\sigma_{\theta_i} = \sigma_x$  in Eq. (1)) for the first SDF and  $\pi/2$  (corresponding to  $\sigma_{\theta_i} = \sigma_y$ ) for the second

SDF. The resulting spin-phonon Hamiltonian becomes,

$$H = H_x + H_y,$$

where,

$$\begin{aligned} H_x &= \sum_{i,m} \eta_{im} \Omega_i^x \cos(\mu_1 t + \psi_i^x) (\hat{a}_m e^{-i\omega_m t} + h.c.) \sigma_x^i, \\ H_y &= \sum_{i,m} \eta_{im} \Omega_i^y \cos(\mu_2 t + \psi_i^y) (\hat{a}_m e^{-i\omega_m t} + h.c.) \sigma_y^i. \end{aligned} \quad (4)$$

Here,  $\Omega_i^x$  and  $\Omega_i^y$  are Rabi frequencies, and  $\psi_i^x$ ,  $\psi_i^y$  are motional phases corresponding to the 2 SDFs respectively. Again, if we operate each of the two forces in the slow regime ( $|\mu_1 - \omega_m| \gg \eta_{im} \Omega_i^x$ ,  $|\mu_2 - \omega_m| \gg \eta_{im} \Omega_i^y$ ), the first term in the Magnus expansion is negligible [4] and the evolution operator arising from the second term in the Magnus expansion becomes,

$$\begin{aligned} U(\tau) &= \exp \left( -\frac{1}{2} \int_0^\tau dt_1 \int_0^{t_1} dt_2 [H(t_1), H(t_2)] \right) \\ &= \exp \left( -i\tau \sum_{i<j} J_{ij}^x \sigma_x^i \sigma_x^j - i\tau \sum_{i<j} J_{ij}^y \sigma_y^i \sigma_y^j \right. \\ &\quad \left. + \sum_{i<j} \Lambda_{ij}(\tau) \sigma_x^i \sigma_y^j + \sum_i \hat{\zeta}_i(\tau) \sigma_z^i \right). \end{aligned} \quad (5)$$

Where,

$$\begin{aligned} J_{ij}^x &= \Omega_i^x \Omega_j^x \frac{\hbar(\delta\vec{k})^2}{2M} \sum_m \frac{b_{im} b_{jm}}{\mu_1^2 - \omega_m^2}, \\ J_{ij}^y &= \Omega_i^y \Omega_j^y \frac{\hbar(\delta\vec{k})^2}{2M} \sum_m \frac{b_{im} b_{jm}}{\mu_2^2 - \omega_m^2}. \end{aligned} \quad (6)$$

The first two terms in the exponent in Eq. (5) come from  $[H_{x(y)}(t_1), H_{x(y)}(t_2)]$ , and result in the desired spin-spin interactions. The last two terms come from the cross terms, i.e.  $[H_{x(y)}(t_1), H_{y(x)}(t_2)]$ , and lead to an undesirable spin-phonon coupling. For  $\mu_1 = \mu_2$ , the single frequency SDF can be rewritten with a different spin phase, as can be seen from Eq. (4), and therefore the resulting effective spin-spin Hamiltonian is Ising type ( $\sigma_\theta^i \sigma_\theta^j$ ) (Fig. 1(b)). For  $\mu_1 \neq \mu_2$ , there is no secular term in  $\Lambda_{ij}(\tau)$  and  $\hat{\zeta}_i(\tau)$ , however, they may have non-trivial oscillatory terms (see appendix). As  $|\mu_1 - \mu_2|$  is increased beyond zero, the contribution of the oscillatory terms diminishes (Fig. 1(c)), and the evolution becomes consistent with an effective XY-type Hamiltonian (Fig. 1(d)),

$$H_{\text{eff}} = \hbar \sum_{i<j} J_{ij}^x \sigma_x^i \sigma_x^j + \hbar \sum_{i<j} J_{ij}^y \sigma_y^i \sigma_y^j, \quad (7)$$

when,

$$|\mu_1 - \mu_2| \gg \max_{i,j} (|J_{ij}^x|), \quad |\mu_1 - \mu_2| \gg \max_{i,j} (|J_{ij}^y|). \quad (8)$$

In the following section, we provide experimental validation of the above analysis.

The experiments are performed on  $^{171}\text{Yb}^+$  ions in a four-rod Paul trap with trap frequencies  $\omega_X \approx 2\pi \times 1.135$  MHz,  $\omega_Y \approx 2\pi \times 0.920$  MHz and  $\omega_Z \approx 2\pi \times 201$  kHz. The spins are encoded in the two hyperfine ‘clock’ states,  $S_{1/2} |F=0, m_F=0\rangle$  ( $|\downarrow\rangle$ ) and  $S_{1/2} |F=1, m_F=0\rangle$  ( $|\uparrow\rangle$ ), of the  $^{171}\text{Yb}^+$  ions, separated in energy by the hyperfine splitting  $\omega_{\text{hf}}/2\pi = 12.643$  GHz. Here,  $F$  and  $m_F$  are quantum numbers representing the total atomic angular momentum and its projection along a weak magnetic field of around 3.5 G.

We perform coherent operations on the ions, through 2-photon Raman transitions with a 355 nm pulsed laser with a repetition rate of 80 MHz [23]. The wave-vector difference of the two Raman beams,  $\delta\vec{k}$ , is oriented such that we can excite phonon modes along both transverse trap axes,  $X'$  and  $Y'$  (Fig. 2(a)). We modulate the frequency of the Raman 1 beam with four harmonic tones to create four beatnotes driving SDFs at two frequencies  $\mu_1 = \omega_{\text{TILT}}^{X'} - 2\pi \times 8$  kHz,  $\mu_2 = \omega_{\text{TILT}}^{X'} - 2\pi \times 5$  kHz respectively (Fig. 2(b)). Here,  $\omega_{\text{COM}}^{X'} = \omega_X$  and  $\omega_{\text{TILT}}^{X'} = 2\pi \times 1.117$  MHz are the frequencies of the COM and TILT modes in the  $X'$  direction respectively. The SDF detunings are chosen to be smaller than the separation between the modes to minimize the contribution from all modes except the  $X'$  TILT mode.

The experimental sequence is as follows. We apply 1.5 ms of Doppler cooling and 8 ms of Raman sideband cooling to cool all transverse modes to  $\bar{n} < 1$  to be in the Lamb-Dicke regime, and global optical pumping for 20  $\mu\text{s}$  to initialize in  $|\downarrow\downarrow\rangle$  state. An optional  $\pi$ -pulse driven by microwave radiation (at frequency  $\omega_{\text{hf}}$ ) and a site-selective optical pumping (that maintains the coherence of the neighboring ion with  $\sim 99.9\%$  fidelity [24]) can alternatively prepare the initial states  $|\downarrow\uparrow\rangle$  and  $|\uparrow\downarrow\rangle$ . The spin-dependent forces are then applied (Eq. (4)) for a pulse duration  $\tau$ .

We finally measure the spin states by state-dependent fluorescence on a photo-multiplier tube (PMT) for 1.5 ms. We calibrate the fluorescence counts by preparing the spins in  $|\uparrow\uparrow\rangle$  with a microwave  $\pi$ -pulse in a separate experiment and obtain approximately 80 PMT counts for this state. Since global fluorescence measurements cannot distinguish between  $|\uparrow\downarrow\rangle$  and  $|\downarrow\uparrow\rangle$  states, we apply a local optical pumping pulse on the first ion just before the measurement to convert it to a single ion measurement, when necessary.

Figure 2(c) shows the spin dynamics when initialized in  $|\downarrow\downarrow\rangle$  state. As in the numerical simulations Fig. 1, we tune the Rabi frequencies to achieve  $J_{12}^x \approx J_{12}^y$  to get an effective XY model when the interactions are mediated simultaneously. We set the Rabi frequencies,  $\Omega_i^x = 2\pi \times 15$  kHz and  $\Omega_i^y = 2\pi \times 11.5$  kHz (approximately equal between the two ions). With  $H_x$  and  $H_y$  applied separately, we observe oscillations between  $|\downarrow\downarrow\rangle$  and  $|\uparrow\uparrow\rangle$ , as expected. We estimate  $J_{12}^x = 2\pi \times 77(2)$  Hz and  $J_{12}^y =$

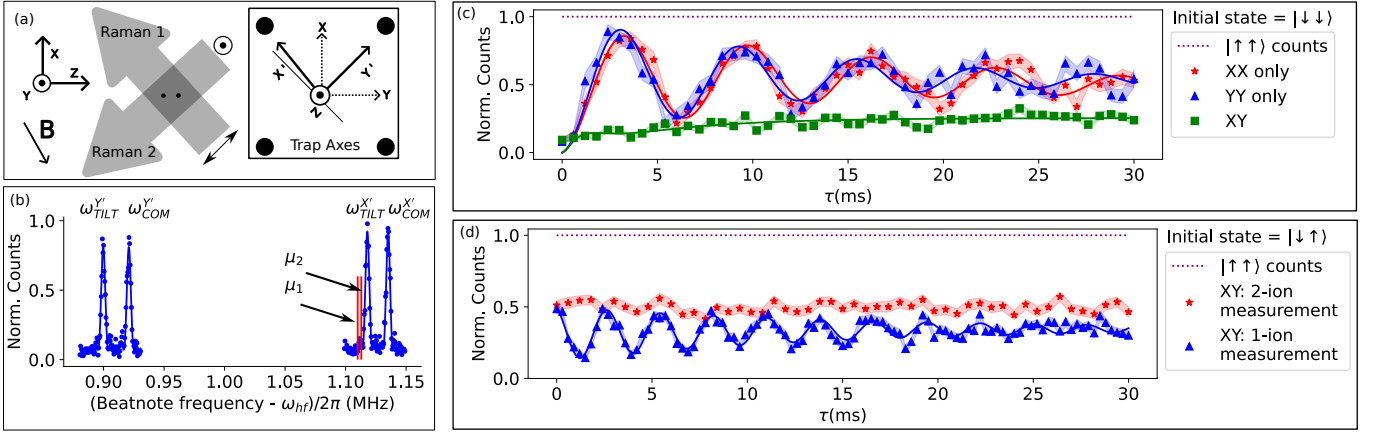


FIG. 2. **Experimental observation of dynamics under the XY Hamiltonian.** (a) Relative orientations of 2 raman beams w.r.t. ions (black dots), magnetic field, and beam polarization. The inset shows the transverse trap axes,  $X'$  and  $Y'$  in the XY plane with the circles representing the electrode (rod) positions. The k-vector difference  $\delta\vec{k}$  between the Raman beams lies along the X-axis and hence the Raman beams can excite both  $X'$  and  $Y'$  motional modes. Experimental data are presented in (b)-(d), where the fluorescence counts are normalized w.r.t. the counts from the  $|\uparrow\uparrow\rangle$  state in each experimental repetition and each point is the average of 100 experimental repetitions. (b) Raman beatnote frequency scan with 2 ions showing the blue sidebands. The higher frequency modes correspond to the  $X'$  direction. We have,  $\omega_{COM}^{X'} = 2\pi \times 1.135$  MHz,  $\omega_{TILT}^{X'} = 2\pi \times 1.117$  MHz,  $\omega_{COM}^{Y'} = 2\pi \times 0.920$  MHz,  $\omega_{TILT}^{Y'} = 2\pi \times 0.899$  MHz,  $\mu_1 = \omega_{TILT}^{X'} - 2\pi \times 8$  kHz,  $\mu_2 = \omega_{TILT}^{X'} - 2\pi \times 5$  kHz. For (c) and (d), solid lines represent fit to  $f(\tau)_{T,\alpha,\beta,\phi,C} = \sin^2(\omega\tau + \phi)(\alpha e^{-\tau/T}) + \beta(1 - e^{-\tau/T}) + C$  and the shaded regions represent standard error.  $\Omega_i^x \approx 2\pi \times 15$  kHz ( $i = 1, 2$ ) and  $\Omega_i^y \approx 2\pi \times 11.5$  kHz ( $i = 1, 2$ ). (c) When initialized in  $|\downarrow\downarrow\rangle$ , we observe oscillations in the fluorescence counts, when either of the two spin-dependent forces are applied separately (red and blue plots). From the fit parameter  $\omega$ , we estimate  $J_{12}^x = 2\pi \times 77(2)$  Hz and  $J_{12}^y = 2\pi \times 80(3)$  Hz. When the two forces are applied simultaneously (green plots), we observe no appreciable oscillations, as expected from the XY Hamiltonian (see text). (d) Observation of dynamics under the XY Hamiltonian, when initialized in  $|\downarrow\uparrow\rangle$ . The normalized total fluorescence counts from both ions are nearly constant over the evolution time, as the spin states of the ions oscillate out of phase with each other (between  $|\downarrow\uparrow\rangle$  and  $|\uparrow\downarrow\rangle$ ). Oscillations are recovered with a 1-ion fluorescence measurement (see text). We observe oscillations at  $2\pi \times 178(2)$  Hz, which is consistent with the expected oscillation frequency of  $J_{12}^x + J_{12}^y$ , counting for  $\approx 15\%$  drifts in the couplings over the timescale of the data run.

$2\pi \times 80(3)$  Hz. When applied simultaneously, we find no observable oscillations, which is the signature of the XY Hamiltonian, since  $(\sigma_x^1 \sigma_x^2 + \sigma_y^1 \sigma_y^2)|\downarrow\downarrow\rangle = 0$ . The slow increase in the fluorescence counts for the XY Hamiltonian is likely due to the decoherence in the system and slow drifts in the intensity of the laser and the trap frequency (estimated to contribute  $< 15\%$  drift in  $J_{12}^x$  or  $J_{12}^y$ ) over the duration of the data run. To further validate that the  $\sigma_x^i \sigma_x^j$  and the  $\sigma_y^i \sigma_y^j$  couplings are present simultaneously, we initialize the ions in the  $|\downarrow\uparrow\rangle$  state and repeat the experiment. Here, we expect oscillations between the  $|\downarrow\uparrow\rangle$  and the  $|\uparrow\downarrow\rangle$  states, at frequency  $J_{12}^x + J_{12}^y$  (see appendix). With a global detection, we expect the fluorescence counts to be flat as observed in Fig. 2(d). However, with an individual detection on ion 1 (i.e. by pumping one ion before detection), we observe oscillations in the fluorescence counts as expected from oscillations between the  $|\downarrow\uparrow\rangle$  and  $|\uparrow\downarrow\rangle$ . From the data in Fig. 2(d), we observe oscillations at  $2\pi \times 178(2)$  which is within the expected 10% fluctuations of the extracted  $J_{12}^x + J_{12}^y$  from previous experiments.

The inherent full-connectivity of trapped ions allows for the scheme to be readily scalable to a large number of ions like in the case of the tunable Ising interac-

tions [1, 4]. For example, an interaction profile with a power law decay that has been widely studied for quantum Ising models [1] can be extended to XY interactions. To achieve this interaction profile, first the Rabi frequencies ( $\Omega_i^x$ ) and the detuning ( $\mu_1$ ) can be chosen to obey an approximate power law in the coupling matrix  $J^x$  in Eq. (6). Then,  $\mu_2$  can be chosen to satisfy Eq. (8) while keeping it close to  $\mu_1$ , to maintain the same form for  $J^x$  and  $J^y$ . Further, if  $J^x = J^y$  is desired, then  $\Omega_i^x$ s can be calculated using a global scaling w.r.t  $\Omega_i^x$ s to compensate for the unequal  $\mu_1$  and  $\mu_2$ . Figure 3 shows that the interaction profiles along  $x$  and  $y$ -directions match to better than 99% with the global scaling of Rabi frequencies, even when  $|\mu_1 - \mu_2|$  is chosen to be 30 times higher than  $\max(J^x)$ . We find that this approach of scaling the Rabi frequencies works well whenever  $\mu_1(\mu_2)$  is parked close to a motional mode since the contribution to the  $J_{ij}^x$  ( $J_{ij}^y$ ) is dominated by a single motional mode. Note that, Eq. (8) is weaker than the constraint for applying each of the forces in the slow regime ( $|\mu_{1(2)} - \omega_m| \gg \eta_{im}\Omega_i^{x(y)}$ ). This is because, in the slow regime, individual matrix elements  $J_{ij}^x$  ( $J_{ij}^y$ ) are an order of magnitude smaller than  $|\mu_{1(2)} - \omega_m|$  and hence leave enough freedom to satisfy Eq. (8). Thus, by simultaneously applying a pair of SDFs

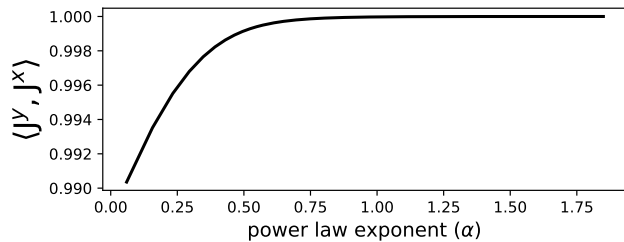


FIG. 3. **Calculated proximity of  $J^x$  and  $J^y$  while engineering power law decay in XY couplings for  $N = 25$  ions.** To have a linear chain of  $N = 25$  ions, we assume trap frequencies of  $\omega'_X = 2\pi \times 5$  MHz,  $\omega'_Y = 2\pi \times 4.8$  MHz and  $\omega_Z = 2\pi \times 400$  kHz.  $J^x$  is calculated using Eq. (7), assuming equal  $\Omega_i^x$  on all ions operating in the regime where  $\max(\{J_{ij}^x\}) \approx 2\pi \times 100$  Hz.  $\mu_1$  is varied from  $\omega_x + 2\pi \times 1$  kHz to  $\omega_x + 2\pi \times 1$  MHz to achieve the approximate power scaling, i.e.,  $J_{ij}^x \approx 1/|i-j|^\alpha$  with  $\alpha \in (0.1, 1.8)$ . To get the  $J_{ij}^y = J_{ij}^x$ , we set  $\mu_2 = \mu_1 + 2\pi \times 3$  kHz and calculate  $\Omega_i^y$  from Eq. (7) by assuming only participation of the closest motional mode i.e., COM. To compare  $J^x$  and  $J^y$  we use the Frobenius norm,  $\langle \mathbf{A}, \mathbf{B} \rangle_F = \text{Tr}(\mathbf{A}^\dagger \mathbf{B})$  after appropriate normalization.

near each motional mode, the full spin-spin interaction profile can be engineered arbitrarily [11, 25]. It should be noted, however, that the calculation of the coupling matrix should take into account any AC Stark shift induced from the spin-dependent forces when the relative scale of the couplings needs to be precisely matched.

In summary, we have demonstrated tunable long-range

XY-type couplings ( $J_{ij}^x \sigma_x^i \sigma_x^j + J_{ij}^y \sigma_y^i \sigma_y^j$ ) by the parallel application of two spin-dependent forces on the same motional modes. Our approach allows for analog quantum simulations of the XY and anisotropic XY models, as the effective Hamiltonian (Eq. (7)) is valid in continuous time. This opens possibilities to study ground state order of frustrated XY-type models, in principle on programmable lattice geometries [10, 11], and investigate exotic quantum phases, such as spin liquids [26]. Further, evolution under the XY Hamiltonian can be interspersed with single spin quantum gates in analog-digital hybrid quantum simulations [27] to investigate dynamical phase transitions, Hamiltonian quenches, and quantum transport. Our demonstration of parallel SDFs on the same motional modes can further be extended to simulate XYZ-type Hamiltonians by adding a  $\sigma_z$ -SDF (readily implemented using the light-shift gate schemes [28]).

## ACKNOWLEDGMENTS

We thank Jingwen Zhu for helping us on the experimental setup. We acknowledge financial support from the Natural Sciences and Engineering Research Council of Canada Discovery (RGPIN-2018-05250) program, Ontario Early Researcher Award, Canada First Research Excellence Fund (CFREF), New Frontiers in Research Fund (NFRF), University of Waterloo, and Innovation, Science and Economic Development Canada (ISED).

- 
- [1] C. Monroe, W. C. Campbell, L.-M. Duan, Z.-X. Gong, A. V. Gorshkov, P. W. Hess, R. Islam, K. Kim, N. M. Linke, G. Pagano, et al., *Rev. Mod. Phys.* **93**, 025001 (2021), URL <https://link.aps.org/doi/10.1103/RevModPhys.93.025001>.
  - [2] R. Blatt and C. F. Roos, *Nature Physics* **8**, 277 (2012), ISSN 1745-2481, URL <https://doi.org/10.1038/nphys2252>.
  - [3] J. J. García-Ripoll, P. Zoller, and J. I. Cirac, *Phys. Rev. A* **71**, 062309 (2005), URL <https://link.aps.org/doi/10.1103/PhysRevA.71.062309>.
  - [4] K. Kim, M.-S. Chang, R. Islam, S. Korenblit, L.-M. Duan, and C. Monroe, *Phys. Rev. Lett.* **103**, 120502 (2009), URL <https://link.aps.org/doi/10.1103/PhysRevLett.103.120502>.
  - [5] K. Mølmer and A. Sørensen, *Phys. Rev. Lett.* **82**, 1835 (1999), URL <https://link.aps.org/doi/10.1103/PhysRevLett.82.1835>.
  - [6] P. Wang, C.-Y. Luan, M. Qiao, M. Um, J. Zhang, Y. Wang, X. Yuan, M. Gu, J. Zhang, and K. Kim, *Nature Communications* **12**, 233 (2021), ISSN 2041-1723, URL <https://doi.org/10.1038/s41467-020-20330-w>.
  - [7] T. P. Harty, D. T. C. Allcock, C. J. Ballance, L. Guidoni, H. A. Janacek, N. M. Linke, D. N. Stacey, and D. M. Lucas, *Phys. Rev. Lett.* **113**, 220501 (2014), URL <https://link.aps.org/doi/10.1103/PhysRevLett.113.220501>.
  - [8] A. Auerbach, *Interacting Electrons and Quantum Magnetism* (Springer New York, NY, 1994), 2nd ed.
  - [9] S. Sachdev, *Quantum Phase Transitions* (Cambridge University Press, 2011), 2nd ed.
  - [10] S. Korenblit, D. Kafri, W. C. Campbell, R. Islam, E. E. Edwards, Z.-X. Gong, G.-D. Lin, L.-M. Duan, J. Kim, K. Kim, et al., *New Journal of Physics* **14**, 095024 (2012), URL <https://dx.doi.org/10.1088/1367-2630/14/9/095024>.
  - [11] Y. H. Teoh, M. Drygala, R. G. Melko, and R. Islam, *Quantum Science and Technology* **5**, 024001 (2020), URL <https://dx.doi.org/10.1088/2058-9565/ab657a>.
  - [12] P. Richerme, Z.-X. Gong, A. Lee, C. Senko, J. Smith, M. Foss-Feig, S. Michalakakis, A. V. Gorshkov, and C. Monroe, *Nature* **511**, 198 (2014), ISSN 1476-4687, URL <https://doi.org/10.1038/nature13450>.
  - [13] P. Jurcevic, B. P. Lanyon, P. Hauke, C. Hempel, P. Zoller, R. Blatt, and C. F. Roos, *Nature* **511**, 202 (2014), ISSN 1476-4687, URL <https://doi.org/10.1038/nature13461>.
  - [14] J. Smith, A. Lee, P. Richerme, B. Neyenhuis, P. W. Hess, P. Hauke, M. Heyl, D. A. Huse, and C. Monroe, *Nature Physics* **12**, 907 (2016), ISSN 1745-2481, URL <https://doi.org/10.1038/nphys3783>.
  - [15] T. G. Kiely and J. K. Freericks, *Phys. Rev. A* **97**, 023611 (2018), URL <https://link.aps.org/doi/10.1103/PhysRevA.97.023611>.

- 1103/PhysRevA.97.023611.
- [16] Z. Davoudi, M. Hafezi, C. Monroe, G. Pagano, A. Seif, and A. Shaw, Phys. Rev. Res. **2**, 023015 (2020), URL <https://link.aps.org/doi/10.1103/PhysRevResearch.2.023015>.
- [17] J. Johansson, P. Nation, and F. Nori, Computer Physics Communications **184**, 1234 (2013), ISSN 0010-4655, URL <https://www.sciencedirect.com/science/article/pii/S0010465512003955>.
- [18] P. J. Lee, K.-A. Brickman, L. Deslauriers, P. C. Haljan, L.-M. Duan, and C. Monroe, Journal of Optics B: Quantum and Semiclassical Optics **7**, S371 (2005), URL <https://dx.doi.org/10.1088/1464-4266/7/10/025>.
- [19] S.-L. Zhu, C. Monroe, and L.-M. Duan, Phys. Rev. Lett. **97**, 050505 (2006), URL <https://link.aps.org/doi/10.1103/PhysRevLett.97.050505>.
- [20] D. F. V. James, Applied Physics B **66**, 181 (1998), ISSN 1432-0649, URL <https://doi.org/10.1007/s003400050373>.
- [21] T. Graß and M. Lewenstein, EPJ Quantum Technology **1**, 8 (2014), ISSN 2196-0763, URL <https://doi.org/10.1140/epjqt8>.
- [22] Y. Zhu, A. M. Green, N. H. Nguyen, C. H. Alderete, E. Mossman, and N. M. Linke, *Pairwise-parallel entangling gates on orthogonal modes in a trapped-ion chain* (2023), arXiv:2302.09145.
- [23] R. Islam, W. C. Campbell, T. Choi, S. M. Clark, C. W. S. Conover, S. Debnath, E. E. Edwards, B. Fields, D. Hayes, D. Hucul, et al., Opt. Lett. **39**, 3238 (2014), URL <https://opg.optica.org/ol/abstract.cfm?URI=ol-39-11-3238>.
- [24] S. Motlakunta, N. Kotibhaskar, C.-Y. Shih, A. Vogliano, D. McLaren, L. Hahn, J. Zhu, R. Häblützel, and R. Islam, *Preserving a qubit during adjacent measurements at a few micrometers distance* (2023), arXiv:2306.03075.
- [25] S. Korenblit, D. Kafri, W. C. Campbell, R. Islam, E. E. Edwards, Z.-X. Gong, G.-D. Lin, L.-M. Duan, J. Kim, K. Kim, et al., New Journal of Physics **14**, 095024 (2012), URL <https://dx.doi.org/10.1088/1367-2630/14/9/095024>.
- [26] C. N. Varney, K. Sun, V. Galitski, and M. Rigol, Phys. Rev. Lett. **107**, 077201 (2011), URL <https://link.aps.org/doi/10.1103/PhysRevLett.107.077201>.
- [27] F. Rajabi, S. Motlakunta, C.-Y. Shih, N. Kotibhaskar, Q. Quraishi, A. Ajoy, and R. Islam, npj Quantum Information **5**, 32 (2019), ISSN 2056-6387, URL <https://doi.org/10.1038/s41534-019-0147-x>.
- [28] C. H. Baldwin, B. J. Bjork, M. Foss-Feig, J. P. Gaebler, D. Hayes, M. G. Kokish, C. Langer, J. A. Sedlacek, D. Stack, and G. Vittorini, Phys. Rev. A **103**, 012603 (2021), URL <https://link.aps.org/doi/10.1103/PhysRevA.103.012603>.

## Appendix A: Distinguishing between XX and XY Hamiltonian (2 ions)

If we start with the Hamiltonian  $H = J_{12}^x \sigma_x^1 \sigma_x^2 + J_{12}^y \sigma_y^1 \sigma_y^2$  and the evolution operator  $U$  such that  $U(\tau) = \exp(-iH\tau)$ . It is easy to show that:

- $U |\downarrow\downarrow\rangle = \cos(\tau(J_{12}^x - J_{12}^y)) |\downarrow\downarrow\rangle - i \sin(\tau(J_{12}^x - J_{12}^y)) |\uparrow\uparrow\rangle$
- $U |\uparrow\uparrow\rangle = \cos(\tau(J_{12}^x - J_{12}^y)) |\uparrow\uparrow\rangle - i \sin(\tau(J_{12}^x - J_{12}^y)) |\downarrow\downarrow\rangle$
- $U |\downarrow\uparrow\rangle = \cos(\tau(J_{12}^x + J_{12}^y)) |\downarrow\uparrow\rangle - i \sin(\tau(J_{12}^x + J_{12}^y)) |\uparrow\downarrow\rangle$
- $U |\uparrow\downarrow\rangle = \cos(\tau(J_{12}^x + J_{12}^y)) |\uparrow\downarrow\rangle - i \sin(\tau(J_{12}^x + J_{12}^y)) |\downarrow\uparrow\rangle$

For the case of the XY Hamiltonian, we have that  $J_{12}^x = J_{12}^y$ . When initialized in  $|\downarrow\downarrow\rangle$ , we do not expect to see oscillations between  $(|\downarrow\downarrow\rangle, |\uparrow\uparrow\rangle)$ . But when initialized in  $|\downarrow\uparrow\rangle$ , we expect to see oscillations between  $(|\downarrow\uparrow\rangle, |\uparrow\downarrow\rangle)$  at a frequency of  $(J_{12}^x + J_{12}^y)$ .

## Appendix B: Detailed derivation of constraint in Eq. (8)

After RWA to Eq. (4) and with  $\delta_{xm} = \omega_m - \mu_1$  and  $\delta_{ym} = \omega_m - \mu_2$  we have,

$$\begin{aligned} H_x &= \sum_{i,m} \eta_{im} \Omega_i^x (a_m e^{-i(\delta_{xm}t + \psi_x)} + h.c.) \sigma_x^i, \\ H_y &= \sum_{i,m} \eta_{im} \Omega_i^y (a_m e^{-i(\delta_{ym}t + \psi_y)} + h.c.) \sigma_y^i \end{aligned} \quad (B1)$$

The first two terms in the exponent of (5) come from calculations already described in [4]. The last two terms come from the cross commutators,

$$\begin{aligned} [H_x(t_1), H_y(t_2)] + [H_y(t_1), H_x(t_2)] &= \left[ \sum_{i,m} \eta_{im} \Omega_i^x (a_m e^{-i(\delta_{xm}t_1 + \psi_x)} + h.c.) \sigma_x^i, \sum_{j,n} \eta_{jn} \Omega_j^y (a_n e^{-i(\delta_{yn}t_2 + \psi_y)} + h.c.) \sigma_y^j \right] \\ &+ \left[ \sum_{i,m} \eta_{im} \Omega_i^y (a_m e^{-i(\delta_{ym}t_1 + \psi_y)} + h.c.) \sigma_y^i, \sum_{j,n} \eta_{jn} \Omega_j^x (a_n e^{-i(\delta_{xn}t_2 + \psi_x)} + h.c.) \sigma_x^j \right] \end{aligned}$$

$$\begin{aligned}
&= \sum_{i,m,n} \eta_{im} \eta_{in} \Omega_i^x \Omega_i^y (a_m e^{-i(\delta_{xm} t_1 + \psi_x)} + h.c.) (a_n e^{-i(\delta_{yn} t_2 + \psi_y)} + h.c.) [\sigma_x^i, \sigma_y^i] \\
&+ \sum_{i,m,n} \eta_{im} \eta_{in} \Omega_i^y \Omega_i^x (a_m e^{-i(\delta_{ym} t_1 + \psi_y)} + h.c.) (a_n e^{-i(\delta_{xn} t_2 + \psi_x)} + h.c.) [\sigma_y^i, \sigma_x^i] \\
&+ \sum_{i,j,m} \eta_{im} \eta_{jm} \Omega_i^x \Omega_j^y [(a_m e^{-i(\delta_{xm} t_1 + \psi_x)} + h.c.), (a_m e^{-i(\delta_{ym} t_2 + \psi_y)} + h.c.)] \sigma_x^i \sigma_y^j \\
&+ \sum_{i,j,m} \eta_{im} \eta_{jm} \Omega_i^y \Omega_j^x [(a_m e^{-i(\delta_{ym} t_1 + \psi_y)} + h.c.), (a_m e^{-i(\delta_{xm} t_2 + \psi_x)} + h.c.)] \sigma_y^i \sigma_x^j \\
&= 2i \sum_{i,m,n} \eta_{im} \eta_{in} \Omega_i^x \Omega_i^y (a_m e^{-i(\delta_{xm} t_1 + \psi_x)} + h.c.) (a_n e^{-i(\delta_{yn} t_2 + \psi_y)} + h.c.) \sigma_z^i \\
&- 2i \sum_{i,m,n} \eta_{im} \eta_{in} \Omega_i^y \Omega_i^x (a_m e^{-i(\delta_{ym} t_1 + \psi_y)} + h.c.) (a_n e^{-i(\delta_{xn} t_2 + \psi_x)} + h.c.) \sigma_z^i \\
&+ 2i \sum_{i,j,m} \eta_{im} \eta_{jm} \Omega_i^x \Omega_j^y \sigma_x^i \sigma_y^j (\sin(\delta_{ym} t_2 - \delta_{xm} t_1 + \psi_y - \psi_x) - \sin(\delta_{ym} t_1 - \delta_{xm} t_2 - \psi_y + \psi_x))
\end{aligned} \tag{B2}$$

Using the above expressions ( and performing the integrals in Eq. (5) we find that For  $\mu_1 \neq \mu_2$ , there is no secular term in  $\Lambda_{ij}(\tau)$  and  $\hat{\zeta}_i(\tau)$ , however, the oscillatory term in  $\Lambda_{ij}(\tau)$  could get unbounded due to the presence of  $(\delta_{xm} - \delta_{ym})$  in the denominator. Let us define  $\tilde{\Lambda}_{ij}$  to be the coefficient of the largest oscillatory term in  $\Lambda_{ij}(\tau)$ . It can then be shown that

$$|\tilde{\Lambda}_{ij}| \leq \frac{4 \times \max(|J_{ij}^x|, |J_{ij}^y|)}{|\mu_1 - \mu_2|}. \tag{B3}$$

When Eq. (8) is satisfied,  $\tilde{\Lambda}_{ij}$  remains small and the contribution of the cross terms in Eq. (5) becomes negligible and the XY-type couplings remain in the effective Hamiltonian.